Unsupervised Brain Tumor Detection

Anonymous Submission

No Institute Given

Abstract. *Accurate and fast automatic detection of brain tumors in 3D MR neuroimages can significantly aid early diagnosis, surgical planning, and follow-up assessment. Primary and metastatic tumors, which present substantial challenges to both human and state-of-the-art brain tumor detection algorithms due to their diverse location and size, need to be carefully monitored. We present a fully automatic, unsupervised algorithm that can detect single and multiple tumors ranging in size from 3 to 28,079 mm^3. Using 20 clinical 3D MR scans containing 1 to as many as 15 tumors per scan, our proposed approach achieves an 87.84 - 95.30% detection rate and an average end-to-end running time of 4 minutes. In addition, 5 normal clinical 3D MR scans are evaluated quantitatively to demonstrate that our approach also has the potential to discriminate between suspicious and normal brains.*

Key words: *3D separable Laplacian of Gaussian, 3D blob detection, brain tumor detection, MRI brain asymmetry.*

1 Introduction

Accurate and fast automatic brain tumor detection from MR images is an important step for computer aided diagnosis (CAD), optimized treatment, and surgical planning. In order to assess the effectiveness of treatment and decide the next course of action, clinicians are often faced with the task of manually searching sequential follow-up scans of cancer patients for the presence and variation of tumors, both old and new. Existing tumors must be compared for volume change, while newly grown primary lesions must be detected as early as possible. Such tasks become increasing tedious when patients have a large number of tumors. Automatic detection of multiple tumors of varying size can thus be of great assistance in monitoring patient response to treatment. Detection of multiple, small-sized tumors is particularly important since these can indicate potential metastasis or early stage tumors; metastatic brain tumors that originated from elsewhere have more than four times the occurrence rate of primary brain tumors [18]. Detection of such tumors, however, proves challenging for both clinicians, who can suffer from fatigue and poor image quality, and state-of-the-art brain tumor detection algorithms.

The general problem of brain tumor detection has attracted many researchers. The majority of recent related work is made up of supervised learning methods for tumor segmentation [27][3][5][10][20][23][15], where a set of training data with multiple modalities (T1, T2, Flair) is used to train a classifier, and the classifier is then evaluated on test cases to classify the voxels [31][33] or regions [3][5] of a tumor. Supervised methods require excessive computation time for both training and inference; a detailed comparison of prior work from [3] shows that, even with just 10 or fewer 3D images for evaluation, tumor segmentation per image can take hours. Moreover, detection rates for various tumor sizes are not reported.

More recent work has addressed performance on small (early stage) and multiple tumors (metastasis), and the use of features such as shape and the bilateral symmetry of the brain in unsupervised methods has started to emerge [1][2][24][28]. However, such methods are still in their infancy, as their precision and accuracy rates leave much to be improved [1][2][24][28].

We make three major contributions in this paper: (1) An unsupervised hierarchical framework that prunes false positive blobs from tens of thousands to a single digit, with the fastest end-to-end running time (4 minutes) and best detection rates ($87.84 \sim 95.30\%$) reported thus far [1][2]. (2) A novel 3D blob-, compact shape-, and brain asymmetry-based tumor detection algorithm that allows us to bypass the need for full-brain registration, which can be both time consuming and error prone, and detect tumors of varying sizes (3-28079 mm^3). (3) Our blob-based approach allows the use of the final 3D blob count as a feature to discriminate between brains that are tumor-free and abnormal. The detected 3D blobs can also be used as automatic initial seeds for fully automatic 3D brain tumor segmentation.

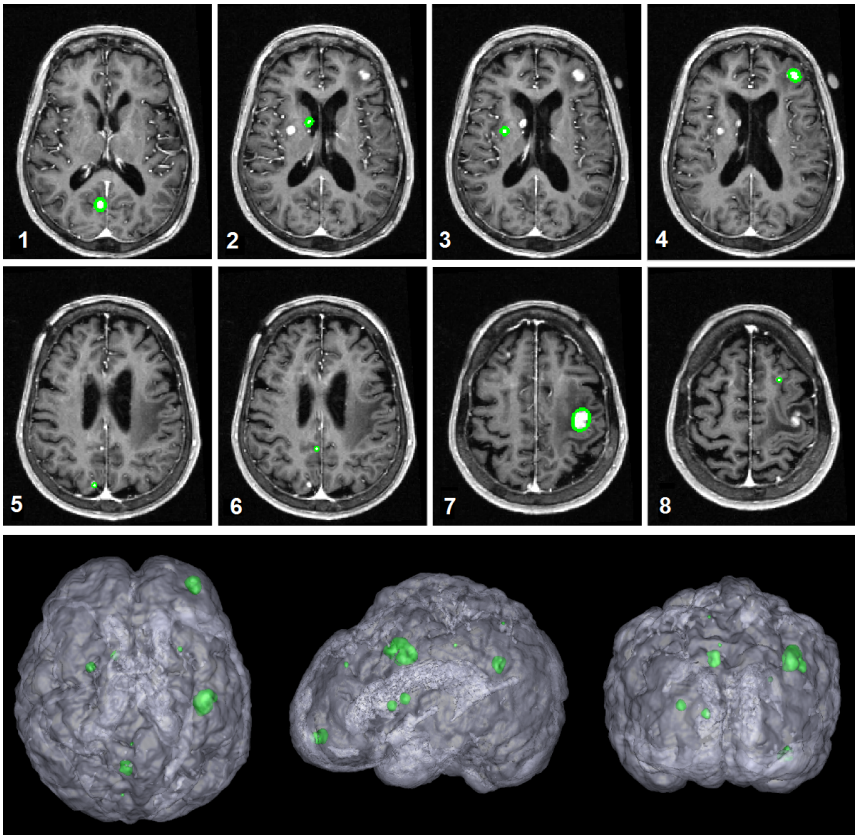

Fig. 1. The result of segmentation of case #11, which had 8 tumors. The first two rows are the 8 tumors detected using the proposed algorithm (circled in green). The 3rd row shows the 3D segmentation result using IFT-Watershed [4] in 3 orientations (axial, sagittal, and coronal).

2 Proposed Method

We propose an unsupervised hierarchical framework for automatically, accurately, and efficiently detecting brain tumors in T1 contrast-enhanced MR images. For a given MR image, our framework finds 3D blobs in the brain and then prunes them in 3 sequential stages—non-maximum supression of 3D blob detection response, blob shape pruning, and bilateral asymmetry pruning—resulting in a final set of tumor candidates (see Fig. 2). 3D blob detection is used for region of interest localization, while blob detection response (B), a blob shape score (S) and the measure of bilateral asymmetry produced by the blob (A) are used as features to determine a thresholding score used to decide whether a given blob is a tumor.

After trying various combinations, C, of our three feature scores, we found that the best is given by:

$$C(B, S, A) = \frac{B + A}{S} \tag{1}$$

We begin by using the observation supported by our medical collaborators that, statistically speaking, brain tumors appear asymmetrically in human brains. Therefore, we first apply a fully automatic midsagittal plane (MSP) extraction algorithm to align the MSP of each 3D brain scan [29]. This enables later asymmetry analysis. We also create a binary map of the volume, with 1s representing brain voxels and 0s representing voxels outside the brain, segmented automatically for the brain-only region (skull-stripping) using FSL [13][14]. This is used to keep only the blobs that are within the boundaries of the brain.

The 3D blob detection response for each detected blob is obtained using a separable 3D Laplacian of Gaussian (LoG) filter, which is described in detail in section 2.2; the shape pruning stage analyzes the compactness of a 3D blob and is explained in section 2.3; the bilateral asymmetry is calculated using Earth-Mover's Distance (EMD) [21] and is described in section 2.4. At each stage of the hierarchy, we apply empirically defined thresholds to decrease excessive false positives. The features of the remaining 3D blobs are combined into a score, C, which is thresholded to produce our algorithm's final tumors. These can then be used as initial seeds to a segmentation algorithm, such as IFT-watershed [4], to segment the precise 3D volume of each tumor.

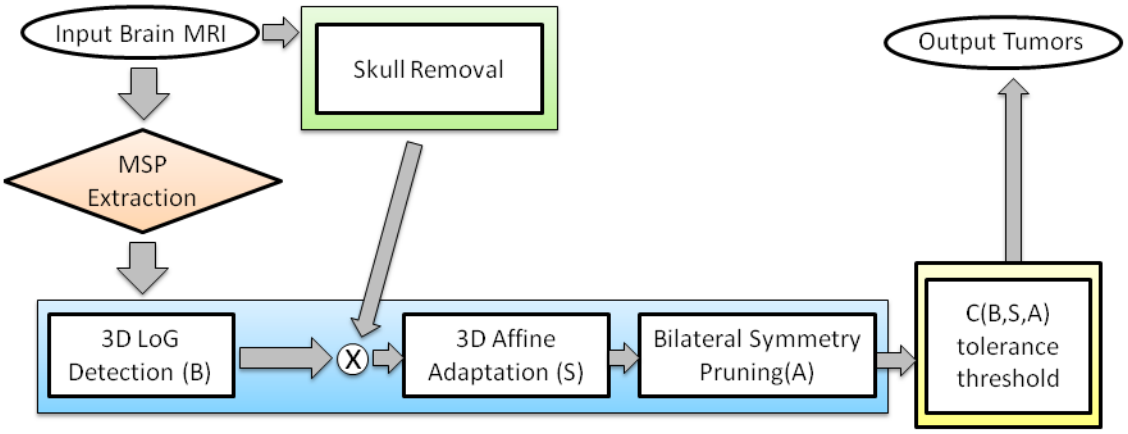

Fig. 2. The hierarchical pruning framework of our proposed method.

2.1 3D Laplacian of Gaussian (LoG) filtering

Because the shape of tumors is usually "blob-like" [25], we propose to use blob detection to automatically and directly generate a pool of tumor candidates from clinical MR neuroimages. In [32], Lindeberg discussed a general formulation of blob detection for N-dimensional space using a Laplacian of Gaussian filter. Based on Lindeberg's scale space-theory [32], we use the Laplacian of Gaussian as a general purpose 3D blob detector, using its 1D separable form for optimized performance and deriving the appropriate scale-space normalizing factor.

We can construct 3D LoG kernels Δg_{xyz} with different scales (σ), and filter a given 3D volumetric image f by Δg_{xyz} to extract 3D blobs at these scales. However, convolution in 3D requires n^3 multiplications per voxel for an $n \times n \times n$ 3D LoG kernel, which is very expensive and time consuming. Decomposition of the 3D convolution into sums of separate 1D convolutions improves the performance significantly.

For the sake of completeness, the formula for separable 3D LoG filtering of 3D volumetric image f as the sum of separate convolutions between 1D Gaussian filters and 1D Laplacian of Gaussian filters is shown as follows:

$$\begin{aligned} h(x,y,z) = & [\,(f \otimes \Delta g_x) \otimes g_y\,] \otimes g_z + \\ & [\,(f \otimes \Delta g_y) \otimes g_x\,] \otimes g_z + \\ & [\,(f \otimes \Delta g_z) \otimes g_x\,] \otimes g_y \end{aligned} \tag{2}$$

where h is the LoG filtered volumetric image f. Eq. 2 shows that 3D LoG filtering can be decomposed and separated into 9 1D LoG filterings. This significantly reduces the multiplications per voxel of 3D LoG from n^3 to just $9n$ and makes general-purpose 3D blob detection using LoG in 3D volumetric data feasible.

Each detected 3D blob's central radius is determined by the scale parameter σ. To find the radius that corresponds to a given scale, we calculate the zero-crossing of the 3D isotropic LoG in polar coordinates:

$$\Delta g_{xyz} = \frac{1}{\sigma^5 2\pi\sqrt{2\pi}} \left(\frac{r^2}{\sigma^2} - 3\right) e^{\frac{-r^2}{2\sigma^2}} \tag{3}$$

Using Eq. 3, the radius, r, of each detected blob can be calculated as follows: $r = \sqrt{3}\,\sigma$.

We are detecting 3D blobs in 10 different scales, and the 3D LoG detection responses must be comparable across these scales. Since the LoG function sums to 0 and its center region sums to -1, the normalizing factor $c(\sigma)$ can be found by integrating over the center region. We solve the integration using spherical polar coordinates:

$$c(\sigma) * \int_{r=0}^{R} \int_{\theta=0}^{2\pi} \int_{\phi=0}^{\pi} \Delta g_{xyz}\, r^2\, sin(\phi)\, d\phi\, d\theta\, dr = -1 \tag{4}$$

The normalizing factor is found to be $c(\sigma) = e^{\frac{3}{2}}\sigma^2/3\sqrt{\frac{6}{\pi}}$, and is thus proportional to σ^2; using this result, the different scales of 3D LoG detection responses can be compared equally weighted by multiplying Eq. 2 by σ^2. If we denote $\theta = (\mu, \sigma^2)$, where μ is the center and σ^2 is the scale of a 3D blob, the normalized 3D blob detection response, B, can be computed as follows:

$$B = \sigma^2 * h(x, y, z|\Theta) \tag{5}$$

Once the volume is filtered by the separable 3D LoG, 5×5×5 non-maximum suppression across scales is applied to the 3D LoG detection responses to eliminate weak interest points.

2.2 Affine Adaptation and Shape Pruning

Besides tumors, the 3D LoG detector may pick up structures like blood vessels, brain linings, ventricles, and skull plates. Since such structures tend to be more elongated in shape than tumors, we prune the detected 3D blobs by applying 3D affine adaptation and discard the ones with highly elliptical shapes as false positives.

For every 3D blob detected, we find the overall gradient direction from the blob's enclosed boundary by finding its structure tensor (a.k.a. the second-moment matrix) in 3 dimensional space:

$$M = \begin{bmatrix} I_x^2 & I_x I_y & I_x I_z \\ I_x I_y & I_y^2 & I_y I_z \\ I_x I_z & I_y I_z & I_z^2 \end{bmatrix} \tag{6}$$

where I_x, I_y, and I_z denote the gradient information along one of the three dimensions x, y, or z. Eigenvalue decomposition is then applied to the structure tensor matrix M, allowing us to obtain eigenvalues $(\lambda 1, \lambda 2, \lambda 3)$ and eigenvectors $(\vec{u1}, \vec{u2}, \vec{u3})$ from the decomposition. The eigenvalues represent the 3D elliptical shape of each 3D blob, whereas the eigenvectors give the rotational information in 3D.

The affine adapted shape score, S from Eq. 1, is then calculated as the ratio of the 3D blob's shortest and longest axes:

$$S = \frac{min(\lambda 1, \lambda 2, \lambda 3)}{max(\lambda 1, \lambda 2, \lambda 3)} \tag{7}$$

2.3 Bilateral Symmetry-based Pruning

Normal human brains exhibit an approximate bilateral symmetry [12]. A key observation in this work is that it is unlikely that brain tumors appear in a way that preserves this symmetry. Availability of algorithms that extract the midsagittal plane (MSP) from neuroimages [29] makes automatic detection of asymmetry-producing 3D blobs in a brain scan possible. Blobs that preserve a high degree of bilateral brain symmetry are discarded as normal brain structures during pruning.

To determine asymmetry produced by a 3D blob, we use Earth-Mover's distance to compare the blob to its bilaterally symmetrical location with respect to the MSP. Earth-Mover's distance (EMD) was introduced by Rubner *et al*, who applied it to image retrieval [21]. Here, we use EMD as a metric to compare how similar the enclosed cumulative intensity distribution, $I(b)$, of a 3D blob is to that of its reflectionally symmetrical location, $I(ref(b))$.

Note that both $I(b)$ and $I(ref(b))$ are 1D distributions, and applying Mallow's distance in 1D is equivalent to using EMD [19]. This allows the computation to run in linear time [6]. Mallow's distance, $M(x, y)$, between cumulative distribution functions x and y can be defined as

$$M(x, y) = \frac{1}{n} \sum_{i=1}^{n} |x_i - y_i| \tag{8}$$

For our purposes, $n = 256$ since there are 256 total grey-scale intensity levels in our images. We define the asymmetry score A of a given 3D blob as:

$$A = M(I(b), I(ref(b))) \tag{9}$$

3 Experiments and Results

We validate our 3D blob-based method for detecting the locations and volumes of tumors using 20 clinical 3D brain MR images with tumors and 5 normal cases. The 25 scans are of single T1 modality with gadolinium enhancement, acquired in the axial plane with 1 mm slice thickness using a Philips Intera 1.5 Tesla Magnet scanner.

Among the 20 abnormal brains, there is a total of 85 tumors that are 2 - 38 mm in diameter (3 - 28731 mm^3 in volume). Both primary and metastatic tumors of various sizes are present with both homogeneous and heterogeneous necrotic cores. This dataset is similar to that used in [2], where tumors were 2 - 45 mm in diameter, and in [1], where tumors were 2.6 - 49.4 mm in diameter.

3.1 Evaluation

We evaluate our algorithm on 20 clinical cases using precision and recall rates. Our precision rate is the ratio of detected blobs that are tumors to all detected blobs, while our recall rate is the ratio of detected tumors to all true tumors. We qualitatively consider a *True Positive* (T_p) to be an extracted region that overlaps the vast majority of a tumor volume, a *False Positive* (F_p) to be an extracted region that overlaps little to none of any part of the tumor volume, and a *False Negative* (F_n) as a tumor region that is not part of any extracted blobs. Precision is thus defined as $T_p/(T_p + F_p)$ and recall is defined as $T_p/(T_p + F_n)$.

The performance of our hierarchical false-positives pruning process is shown in Fig. 3 using 6 different thresholds for C. The plot shows that the pruning stages are able to reduce false positives from extremely high initial numbers ($\sim$ 24,000) to single digits, with a mean end-to-end running time of approximately 4 minutes per 3D MR image. Table 1 shows the quantitative results across the 3 highest thresholds, with the smallest detected tumor being just 3 mm^3. Our results are an improvement over [2], which had an average recall of 89.9% and 34.8 false positives per brain, and [1], which had its highest recall at 90% with $>$1000 false positives per brain. Table 2 shows that the final 3D blob count for the 5 normal brain subjects is lower than the count for subjects with tumors; this shows that blob count can be used as a discriminating feature to help classify normal/abnormal brains.

For nearly all cases, the final detected 3D blob outputs with affine-adapted ellipses already represent good initial estimates of detected brain tumor volumes. For more precise segmentation, our detected blobs can act as automatic initialization regions for many state-of-the-art segmentation methods. To demonstrate this, we apply a watershed method (IFT-Watershed [17]) on cases 15 and 17. With the detected 3D blobs localizing each tumor, we erode each blob to half its size and use the remaining voxels as foreground seeds; similarly we apply dilation using the complementary voxels as background seeds for watershed to segment the tumor volumes. Figure 4 shows the segmentation result, with a Jaccard Coefficient ($T_p/(F_p + T_p + T_n)$) of 90.14% and 85.05% for case 15 and 17, respectively.

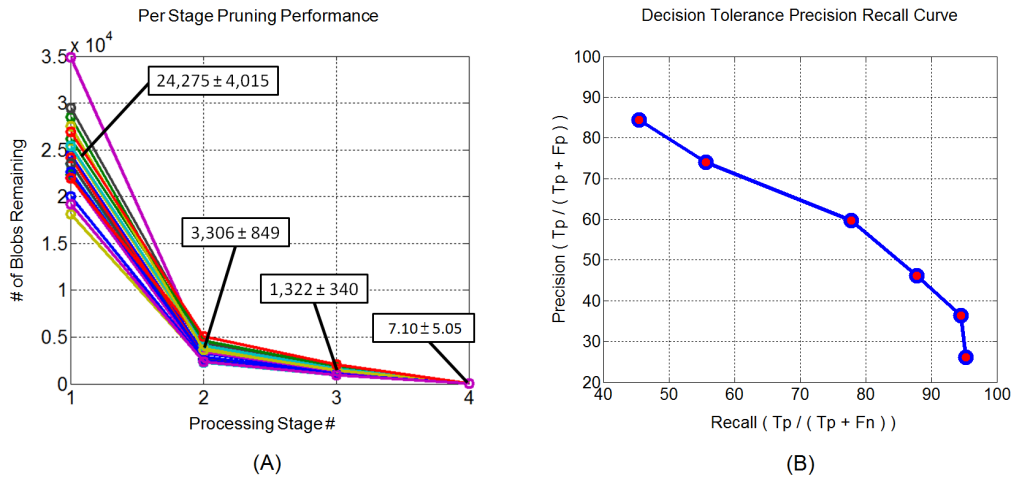

Fig. 3. A: Per stage pruning performance on 20 3D scans. B: The precision-recall curve of the 6 threshold levels for C after the pruning process.

Case Information			Tumor Volume (mm^3)			Top 3 Tolerance Level Results (Tp / Total | Fp)					
Case	Type	# Tumors	Mean	Min	Max	Low		Medium		High	
1	Mets	1	12107	12107	12107	1 / 1	2	1 / 1	2	1 / 1	6
2	Primary	1	1448	1448	1448	1 / 1	3	1 / 1	9	1 / 1	16
3	Mets	2	10809	3532	18086	1 / 2	2	2 / 2	6	2 / 2	8
4	Mets	4	355.25	140	732	4 / 5	2	4 / 5	2	4 / 5	3
5	Mets	11	135.91	4	625	9 / 11	6	9 / 11	8	10 / 11	11
6	Primary	1	11913	11913	11913	1 / 1	2	1 / 1	5	1 / 1	6
7	Mets	15	82.31	3	422	12 / 15	10	14 / 15	15	15 / 15	20
8	Primary	1	2262	2262	2262	1 / 1	2	1 / 1	5	1 / 1	8
9	Mets	1	3723	3723	3723	1 / 1	6	1 / 1	10	1 / 1	12
10	Mets	5	5879	5	28079	4 / 5	2	5 / 5	7	5 / 5	8
11	Mets	8	464.63	18	2226	8 / 8	6	8 / 8	6	8 / 8	8
12	Primary	1	12639	12639	12639	1 / 1	4	1 / 1	5	1 / 1	10
13	Mets	1	22033	22033	22033	1 / 1	2	1 / 1	6	1 / 1	11
14	Mets	1	150	150	150	1 / 1	9	1 / 1	15	1 / 1	18
15	Mets	2	10829	3617	18041	2 / 2	3	2 / 2	8	2 / 2	14
16	Mets	8	602.25	25	2145	4 / 8	1	6 / 8	5	6 / 8	6
17	Mets	5	192.40	12	533	5 / 5	3	5 / 5	6	5 / 5	12
18	Mets	10	572.90	9	3553	6 / 10	3	6 / 10	5	6 / 10	9
19	Mets	2	179.50	56	303	2 / 2	0	2 / 2	0	2 / 2	3
20	Mets	4	487.50	30	1426	3 / 4	6	4 / 4	12	4 / 4	20
Total	-	-	-	-	-	68 / 85	74	75 / 85	137	77 / 85	209
Recall	-	-	-	-	-	87.84±17.47%		94.51±11.23%		95.30±10.92%	
Precision	-	-	-	-	-	46.17±23.44%		35.71±24.18%		26.03±17.78%	
Tp : Fp	-	-	-	-	-	1 : 1.09		1 : 1.83		1 : 2.71	
Final Blobs	-	-	-	-	-	7.10±5.05		10.60±6.02		14.30±6.99	

Table 1. Automatic brain tumor detection results comparing the 3 highest threshold levels for C. The smallest detected tumor is 3 mm^3 from case 5, and the largest detected tumor is 28079 mm^3 from case 10.

4 Conclusion

We have proposed a fully automatic, unsupervised 3D brain tumor detection method. Our average 95.3% detection rate, 10.45 average false positives per brain, and 4 minute run-time (on a standard PC running

Normal	3 Tolerance Level Results (Fp)		
Case	Low	Medium	High
1	1	9	19
2	1	2	8
3	1	6	13
4	0	11	17
5	1	4	5
Avg Final Blobs	0.80±0.45	6.40±3.65	12.40±5.90

Table 2. Automatic brain tumor detection results for normal brains, showing a reduced average final blobs yield specifically with the low threshold for C.

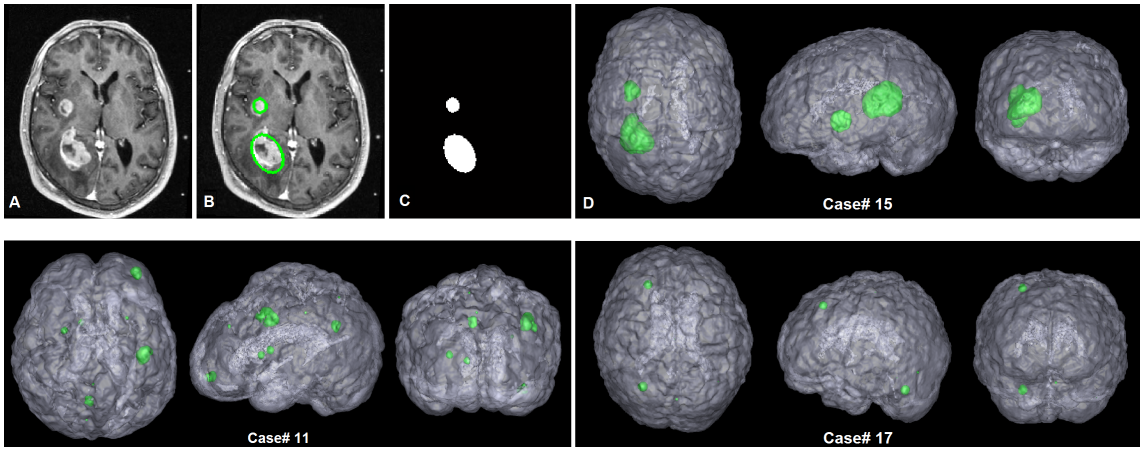

Fig. 4. First row: the 3D segmentation results of case# 15 (2 tumors), visualized using ITK-SNAP [30]. A: case# 15 original image, showing 2 tumors in a representative slice. B: the detection result of our proposed method, note that the blob is 3D, but it is visualized as an affine adapted ellipse in this 2D slice. C: the binary mask from the detected 3D blobs for automatic seeding of watershed segmentation. D: segmentation results with Jaccard Coefficient of 90.14%. Second row: 3D segmentation result for case# 11 (8 tumors) and case # 17 (5 tumors), with Jaccard Coefficient of 87.41% and 85.05%, respectively.

Intel Core i7) are an improvement over state-of-the-art algorithms, which report average detection rates as high as 90% and average false positives per brain as low as 34.8 [1][2]. Our approach uses a simple and effective brain asymmetry-based approach for abnormality detection which can be generalized to many similar applications where the objects have an approximate bilateral symmetry. Our use of the Laplacian of Gaussian to find 3D blobs, which takes under 2 minutes to complete 10 scale levels (compared to the template matching method used in [2], which took about 30 minutes per case) allows our method to be scale-invariant, thus being highly sensitive to any small abnormalities (as small as 3 mm^3). Subsequent affine adaptation and asymmetry-based pruning are able to reduce the number of false positives to single digits. Our final blobs can be used as automatic initialization for tumor delineation using any state-of-the-art segmentation method, as well as a discriminative measure between normal and abnormal brains.

References

1. T. Sugimoto, S. Katsuragawa, T. Hirai, R. Murakami, and Y. Yamashita, "Computerized Detection of Metastatic Brain Tumors on Contrast-Enhanced 3D MR Images by Using a Selective Enhancement Filter." World Congress on Medical Physics and Biomedical Engineering, Vol. 25, pp. 2070-2072, 2010.
2. R. Ambrosini, and P. Wang, "Computer-aided detection of metastatic brain tumors using automated three-dimensional template matching." Journal of Magnetic Resonance Imaging, Vol. 31(1), pp. 85-93, 2010.

3. J.J. Corso, E. Sharon, S. Dube, S. El-Saden, U. Sinha, and A. Yuille, "Efficient Multilevel Brain Tumor Segmentation with Integrated Bayesian Model Classification." IEEE Transactions on Medical Imaging, Vol. 27(5), pp. 629-640, 2008.
4. R. Audigier, and R. A. Lotufo, "Watershed by Image Foresting Transform, Tie-Zone, and Theoretical Relationships with Other Watershed Definitions." In: Proceedings of the 8th International Symposium on Mathematical Morphology, 2007.
5. D. Cobzas, N. Birkbeck, M. Schmidt, M. Jagersand, and A. Murtha, "3D Variational Brain Tumor Segmentation using a High Dimensional Feature Set" International Conference on Computer Vision, 2007.
6. R. Collins, and W. Ge, "CSDD Features: Center-Surround Distribution Distance for Feature Extraction and Matching." European Conference on Computer Vision, 2008.
7. J.J. Corso, E. Sharon, and A. Yuille, "Multilevel Segmentation and Integrated Bayesian Model Classification with an Application to Brain Tumor Segmentation." International Conference on Medical Image Computing and Computer Assisted Intervention, 2006.
8. S. Ho, E. Bullitt, and G. Gerig,"Level set evolution with region competition: Automatic 3-d segmentation of brain tumors." In Proceedings of International Conference on Pattern Recognition, Vol. 1, pp. 532-535, 2002.
9. Q. Yang, and B. Parvin, "CHEF: Convex Hull of Elliptic Features for 3D Blob Detection." International Conference on Pattern Recognition, Vol. 2, 2002.
10. D.T. Gering, "Diagonalized nearest neighbor pattern matching for brain tumor segmentation." International Conference on Medical Image Computing and Computer Assisted Intervention, 2003.
11. K.M. Iftekharuddin, J. Zheng, M.A. Islam, and R.J. Ogg, "Fractal-based brain tumor detection in multimodal MRI." AMC, 2008.
12. S. Joshi, P. Lorenzen, G. Gerig, and E. Bullitt, "Structural and radiometric asymmetry in brain images." Medical Image Analysis, Vol. 7(2), pp. 155-170, 2003.
13. S.M. Smith, "Fast robust automated brain extraction." Human Brain Mapping, Vol. 17(3), pp.143-155, 2002.
14. M. Jenkinson, M. Pechaud, and S. Smith, "BET2: MR-based estimation of brain, skull and scalp surfaces." In Eleventh Annual Meeting of the Organization for Human Brain Mapping, 2005.
15. C.H. Lee, R. Greiner, and M. Schmidt, "Support vector random fields for spatial classification." In: PKDD, pp. 121-132, 2005.
16. S.J. Cotterill, S. Ahrens, M. Paulussen, H.F. Jurgens, P.A. Voute, H. Gadner, and A.W. Craft, "Prognostic factors in Ewing's tumor of bone: analysis of 975 patients from the European Intergroup Cooperative Ewing's Sarcoma Study Group." Journal of Clinical Oncology, Vol. 18(17), pp. 3108-3114, 2000.
17. R. Lotufo, and A. Falcao, "The ordered queue and the optimality of the watershed approaches." In: Mathematical Morphology and its Applications to Image and Signal Processing, Vol. 18, pp. 341-350, 2000.
18. Central Brain Tumor Registry of the United States (CBTRUS) Report, "Primary Brain and Central Nervous System Tumors Diagnosed in the United States in 2004-2006" Feb 2010.
19. E. Levina, and P. Bickel, "The Earth Mover's Distance is the Mallows Distance: Some Insights From Statistics." IEEE International Conference on Computer Vision, Vol. 2, pp. 251-256, 2001.
20. C.H. Lee, S. Wang, A. Murtha, M.R.G. Brown, and R. Greiner, "Segmenting Brain Tumors using Pseudo-Conditional Random Fields." International Conference on Medical Image Computing and Computer Assisted Intervention, 2008.
21. Y. Rubner, C. Tomasi, and L. Guibas, "The Earth Mover's Distance as a Metric for Image Retrieval." International Journal of Computer Vision, Vol. 40(2), pp. 99-121, 2000.
22. G. Moonis, J. Liu, J. Udupa, and D. Hackney, "Estimation of Tumor Volume with Fuzzy-Connectedness Segmentation of MR Images." American Journal of Neuroradiology, Vol. 23, pp. 356-363, 2002.
23. M. Prastawa, E. Bullitt, and G. Gerig, "A Brain Tumor Segmentation Framework Based on Outlier Detection." Medical Image Analysis, Vol. 150, 2004.
24. N. Ray, B. Saha, and M. Brown, "Locating Brain Tumors from MR Imagery Using Symmetry." ACSSC, 2007.
25. M. Prastawa, E. Bullitt, and G. Greig, "Simulation of brain tumors in MR images for evaluation of segmentation efficacy." Medical Image Analysis, Vol. 13(2), pp. 297-311, 2009.
26. M. Schmidt, I. Levner, R. Greiner, A. Murtha, and A. Bistritz, "Segmenting brain tumors using alignment-based features." Machine Learning and Applications, 2005.
27. J. Zhang, K. Ma, M. Er, and V. Chong, "Tumor Segmentation from Magnetic Resonance Imaging by Learning via One-Class Support Vector Machine." International Workshop on Advanced Image Technology, 2004.
28. M. Mancas, B. Gosselin, and B. Macq, "Fast and automatic tumoral area localization using symmetry." IEEE International Conference on Acoustics, Speech and Signal Processing, Vol. 2, pp. 725-728, 2005.
29. G. Ruppert, L. Teverovskiy, C. Yu, A.X. Falcao, and Y. Liu, "A Comparison Study of Neuroimage Midsagittal Plane Extraction Algorithms." PSU CSE Technical Report 09-014, CMU Robotics Institute Technical Report TR-09-43, 2009.
30. P.A. Yushkevich, J. Piven, H.C. Hazlett, R.G. Smith, S. Ho, J.C. Gee, and G. Gerig, "User-guided 3D active contour segmentation of anatomical structures: Significantly improved efficiency and reliability." Neuroimage, Vol. 31(3), pp. 1116-28, 2006.
31. M. Prastawa, E. Bullitt, N. Moon, K. V. Leemput, and G. Gerig, "Automatic brain tumor segmentation by subject specific modification of atlas priors." Academic Radiology, Vol. 10, pp. 1341-1348, 2003.
32. T. Lindeberg, "Feature Detection with Automatic Scale Selection." International Journal of Computer Vision, Vol. 30(2), pp. 79-116, 1998.
33. M. Kaus, S. Warfield, A. Nabavi, P. M. Black, F. A. Jolesz, and R. Kikinis, "Automated segmentation of MR images of brain tumors." Radiology, Vol. 218, pp. 586-591, 2001.